Network Modeling of an Aperture Coupling Between Microstrip Line and Patch Antenna for Active Array Applications

XUANZHENG GAO AND KAI CHANG, SENIOR MEMBER, IEEE

Abstract—**An analytical method based upon the aperture coupling theory and the derivation of S-parameter matrix has been developed for modeling a microstrip line coupled to a microstrip patch antenna using a circular coupling aperture. Closed-form solutions were derived for scattering parameters of the coupling circuit. Input impedance and matching condition can be calculated from the equivalent six-port network. The theoretical results agree well with the measurements. The analysis should have many applications in active array and spatial power combining systems.**

I. INTRODUCTION

RECENT DEVELOPMENTS in microwave and millimeter-wave solid-state devices and integrated circuits have made it possible to implement active devices directly behind a planar antenna element [1]–[3]. Many of these antenna elements and devices can be combined to form an active array. These techniques are compatible with future monolithic implementation by fabricating both passive and active elements on semiconductor substrates. The developments should have many applications in phased array and spatial power combining systems. [4], [5].

One practical difficulty with active arrays is in isolating the input and output signals and maintaining the stability of the array. Another problem is to maintain unidirective radiation and to avoid spurious feed radiation. For monolithic implementation, the use of GaAs substrate for printed dipoles and microstrip patches could have poor performance since GaAs substrate has a high dielectric constant [3].

To overcome these problems, a two-sided substrate circuit has been proposed [3]. As shown in Fig. 1, the active circuits, which include the oscillators, amplifiers, and phase shifters, are fabricated on GaAs substrate located on one side of the ground plane. The antenna elements are fabricated on low-dielectric-constant substrate located on the other side of the ground plane. The coupling between the two layers is accomplished by a circular coupling aperture on the ground plane. The ground plane separates the radiating aperture from the feed network, eliminating the possibility of spurious signal radiation from the source.

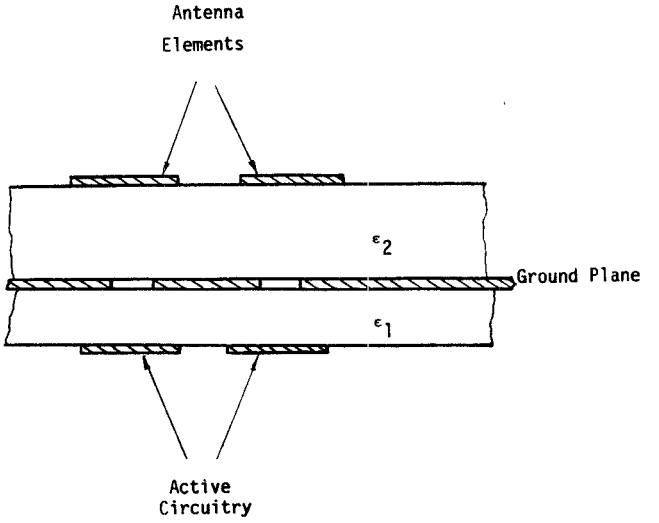

Fig. 1. Two-layer active array.

Recently, Sullivan and Schaubert [6] and Pozar [7] have analyzed the aperture coupled microstrip antenna using a rectangular slot. Their methods are based on a numerical moment method to find the surface electric and magnetic currents. For a round aperture, the selection of base functions could be very difficult and complicated.

This paper reports an analysis and modeling of microstrip line coupled to microstrip patch antenna through a round aperture. The analysis is based upon the aperture coupling theory and the S-parameter matrix derivation. Closed-form solutions were derived for scattering parameters of the equivalent six-port network which are easy to use for actual circuit design. The analysis includes the effects of ground plane thickness and field variation in the aperture. Aperture sizes comparable to the width of the microstrip line can be accommodated.

Manuscript received June 4, 1987; revised September 9, 1987.

X. Gao is with the Xian Radio Technology Institute, China. From September 1985 to August 1987 he was a Visiting Scholar with the Department of Electrical Engineering, Texas A & M University, College Station, TX.

K. Chang is with the Department of Electrical Engineering, Texas A & M University, College Station, TX 77843-3128.

IEEE Log Number 8718368.

0018-9480/88/0300-0505$01.00 ©1988 IEEE

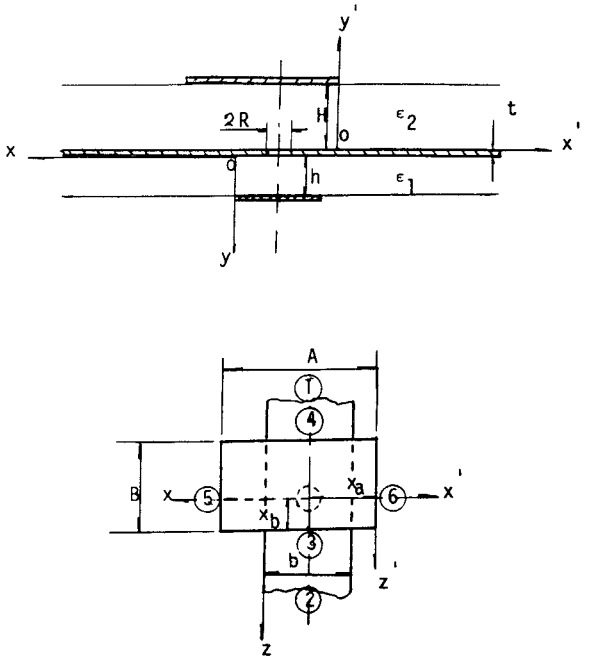

Fig. 2. Geometry of a microstrip coupled to a patch antenna.

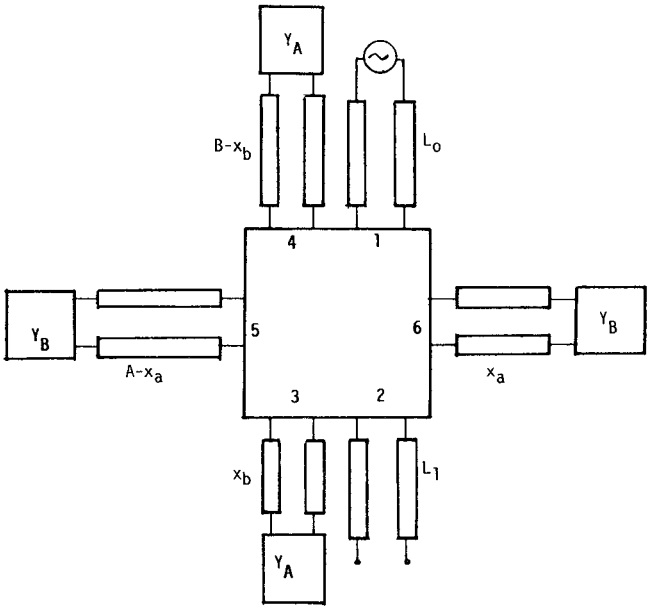

Fig. 3. S-parameter equivalent network.

II. Circuit Configuration

The circuit to be modeled is shown in Fig 2. It is a six-port network. The different parameters are defined below:

(x', y', z'): patch coordinate system

(x, y, z): microstrip line coordinate system

b, h: width and substrate thickness of the microstrip line

A, B, H: width, length, and substrate thickness of the patch antenna

R, x_a, x_b: radius and positions of the aperture

ϵ_1, ϵ_2: relative dielectric constant

t: thickness of the ground plate.

Since the patch radiation occurs at the ends with terminated admittance Y_A and Y_B, the part of the patch from the feed point to the ends can be considered as two microstrip transmission lines with width B and A, and length x_a, $A - x_a$, x_b, and $B - x_b$. The equivalent aperture coupling network between the microstrip line and patch can be represented by the six-port circuit shown in Fig. 3. All reference planes of the ports are taken at the center of the coupling aperture. The normalized S parameter is defined as

$$S_{ij} = \frac{V_i}{V_j} \tag{1}$$

where V_j and V_i are the normalized input wave voltage of the jth port and the scattered wave voltage of the ith port, respectively. The amplitude is determined by the following identity:

$$\frac{1}{2}|V_i|^2 = \frac{1}{2}\mathrm{Re}\left[\int_{s_i} \vec{E}_i \times \vec{H}_i \, ds\right] \tag{2a}$$

$$\frac{1}{2}|V_j|^2 = \frac{1}{2}\mathrm{Re}\left[\int_{s_j} \vec{E}_j \times \vec{H}_j \, ds\right]. \tag{2b}$$

The phase is identical to the scattered field $\vec{E}_i$ and input field $\vec{E}_j$. The integration is carried out over the transmission line cross section.

III. Electromagnetic Fields in Microstrip Transmission Line

The electric and magnetic fields under the microstrip line need to be calculated before the polarizability factors can be determined. For simplicity, we assume a quasi-TEM wave approximation. This assumption is good for thin substrate and low frequency. The electric field can be found using a conformal mapping method [8]. A half infinite z plane of microstrip section is transformed into a half circular image plane $w(z)$. The electric and magnetic fields under the microstrip can be found as

$$E(z) = E_0/[w(z)+1]^* \tag{3a}$$

$$H(z) = \frac{E(z)}{Z}\frac{h}{b} \tag{3b}$$

$$Z = \frac{\pi}{2}\sqrt{\frac{\mu}{\epsilon}}\frac{1}{\ln\left(\frac{r_B}{r_A}\right)} \tag{3c}$$

where E_0 is a constant field, Z is the characteristic impedance, and

$$z = x + jy$$

$$w(z) = re^{j\theta}.$$

for each x and y, the image plane coordinates (r, θ) can be determined by the following two equations:

$$F_1(r,\theta) = \ln r + r\cos\theta + 1 - \frac{\pi x}{h} = 0 \tag{4}$$

and

$$F_2(r,\theta) = r\sin\theta + \theta - \frac{\pi y}{h} = 0. \tag{5}$$

The variables r_A and r_B are the radii of the image plane half rings, determined by the two roots of the following transformation equation:

$$F(r) = \ln r - r + 1 + \frac{\pi b}{2h} = 0. \tag{6}$$

It should be mentioned that the electric field calculated from (3) is not uniform, but dependent on x and y. This is important in the cases where the aperture is not located at the middle of the microstrip line or where the aperture size is comparable to or larger than the microstrip width.

IV. Scattered Fields Due to Coupling

An aperture in a conducting wall is equivalent to an electric dipole normal to the aperture and having a strength proportional to the normal component of the exciting electric field, plus a magnetic dipole in the plane of the aperture having a strength proportional to the exciting tangential magnetic field. Assume the aperture opening does not severely perturb the exciting field for a small aperture compared to the wavelength, the dipole moments can be calculated by [9], [10]

$$\vec{P} = -\frac{\epsilon_1\epsilon_2\epsilon_0}{\epsilon_1+\epsilon_2}\alpha_e(\vec{n}\cdot\vec{E})\vec{n} \tag{7}$$

$$\vec{M} = -\alpha_m\vec{H}_t \tag{8}$$

where $\vec{n}$ is the unit vector normal to the aperture, and α_e and α_m are the electric and magnetic polarizability, respectively. The results for α_e and α_m for large apertures of finite thickness have been given by Levy as follows [11]:

$$\alpha_e = -\frac{2}{3}R^3\exp\left[\frac{-2\pi A_e t}{\lambda_{ce}}\sqrt{1-\frac{f^2}{f_{ce}^2}}\right]A(E_i,E_j) \tag{9}$$

and

$$\alpha_m = \frac{4}{3}R^3\exp\left[\frac{-2\pi A_m t}{\lambda_{cm}}\sqrt{1-\frac{f^2}{f_{cm}^2}}\right]A(H_i,H_j) \tag{10}$$

where $A_e t$ and $A_m t$ are related to t and R [11], and f_{ce}, λ_{ce}, f_{cm}, and λ_{cm} are the cutoff frequencies and wavelengths for the E_{10} and H_{11} modes in the hole, respectively. Expressions for these parameters as a function of t and R can be found in [11].

$A(E_i, E_j)$ or $A(H_i, H_j)$ are the average factors of field for a large aperture. They equal 1 for a small aperture. The factors can be found by field averaging over the aperture (see the Appendix).

The scattered fields can be written as [12]

$$E_i^+ = \sum_n C_{ni}^+(\vec{e}_n + \vec{e}_{zn}) \qquad \text{for } z>0$$

$$H_i^+ = \sum_n C_{ni}^+(\vec{h}_n + \vec{h}_{zn}) \qquad \text{for } z>0$$

$$E_i^- = \sum_n C_{ni}^-(\vec{e}_n - \vec{e}_{zn}) \qquad \text{for } z<0$$

and

$$H_i^- = \sum_n C_{ni}^-(-\vec{h}_n + \vec{h}_{zn}) \qquad \text{for } z<0.$$

C_{ni}^+ and C_{ni}^- can be found by

$$C_{ni}^+ = -\frac{1}{P_n}\int_V(\vec{e}_n - \vec{e}_{zn})\cdot\vec{J}\,dv \tag{11a}$$

$$C_{ni}^- = -\frac{1}{P_n}\int_V(\vec{e}_n + \vec{e}_{zn})\cdot\vec{J}\,dv \tag{11b}$$

where

$$P_n = 2\int_S \vec{e}_n\times\vec{h}_n\cdot\vec{a}_z\,ds.$$

S is a cross-sectional surface of the transmission line, n indicates various modes that possibly exist in the transmission lines, and $\vec{e}_n$, $\vec{e}_{zn}$, $\vec{h}_n$, and $\vec{h}_{zn}$ represent the transverse and longitudinal components of the electric and magnetic fields, respectively. V is the volume in which current $\vec{J}$ exists. $C_{ni}^{\pm}$ is the mode coupling coefficient at the ith port.

For quasi-TEM mode, we have

$$n = 1$$
$$\vec{e}_{zn} = \vec{h}_{zn} = 0$$
$$e_n = E(z)$$
$$h_n = H(z).$$

The scattered fields in the transmission line 3-4 due to the electric dipole $\vec{P}$ with input at port #1 can be calculated by

$$C_{ne}^+ = C_{ne}^- = -\frac{1}{P_n}\int_V \vec{e}_n\cdot\vec{J}\,dv = -\frac{j\omega}{P_n}\left(\frac{\epsilon_1\epsilon_2\epsilon_0}{\epsilon_1+\epsilon_2}\right)\cdot\alpha_e E_i(x_a)E_j\left(\frac{b}{2}\right) \tag{12}$$

$$P_n = 2\int_S \vec{e}_n\times\vec{h}_n\cdot\vec{a}_z\,ds = \frac{4h_i^3E_0^2}{Z_i\pi b_i}\ln\left[\frac{r_B(k)}{r_A(k)}\right]. \tag{13}$$

Here we replace $\vec{J}$ by $j\omega\vec{P}$ and use the results of (7). The integration of (13) is completed in the image plane [8]. The subscript i indicates the scattered field at ports #3 and #4, and j indicates the excited field at port #1. For example, h_i and b_i are the substrate thickness and line width at port #i. Z_i is the characteristic impedance at port #i. $E_j(b/2)$ is the electric field at port #j with $x = b/2$. $r_A(k)$ and $r_B(k)$ indicate the ring radii of the kth transmission line. For line 1-2, $k=1$; line 3-4, $k=2$; line 5-6, $k=3$.

The scattered fields due to the magnetic dipole can be obtained by

$$C_{nm}^{+} = -C_{nm}^{-} = \frac{j\omega}{P_n}\vec{B}_n^{-}\cdot\vec{M} = \frac{-j\omega}{P_n}\mu_t\alpha_m H_t(x_a)H_J\left(\frac{b}{2}\right). \tag{14}$$

The mode coupling coefficients at port #i are then given by

$$C_{nt}^{+} = C_{ne}^{+} + C_{nm}^{+} = \frac{-j\pi^2}{H^2\lambda_0 E_0^2(H)} \cdot\left(\frac{\epsilon_1\epsilon_2\alpha_e}{\epsilon_1+\epsilon_2}\frac{Z_t}{Z_0}\frac{A}{H} + \frac{Z_0\alpha_m}{Z_J}\frac{h}{b}\right)\frac{E_t(x_a)E_J\left(\frac{b}{2}\right)}{2\ln\left[r_B(2)/r_A(2)\right]} \tag{15a}$$

$$C_{nt}^{-} = C_{ne}^{-} + C_{nm}^{-} = C_{ne}^{+} - C_{nm}^{+} = \frac{-j\pi^2}{H^2\lambda_0 E_0^2(H)} \cdot\left(\frac{\epsilon_1\epsilon_2}{\epsilon_1+\epsilon_2}\frac{Z_t}{Z_0}\frac{A}{H}\alpha_e - \frac{Z_0}{Z_J}\frac{h}{b}\alpha_m\right)\frac{E_t(x_a)E_J\left(\frac{b}{2}\right)}{2\ln\left[r_B(2)/r_A(2)\right]} \tag{15b}$$

where

$$Z_0 = \sqrt{\frac{\mu_0}{\epsilon_0}} = 120\pi.$$

Equations (15) show that the field along the positive z direction is different from the one along the negative z direction; that is, the aperture coupling behaves directionally and it could cause unbalanced feed to the patch. Similarly, except that $C_{nm}^{\pm} = 0$ due to $\vec{B}_n$ perpendicular to $\vec{M}$, the scattered fields in transmission line 5-6 with input at port 1 are given by

$$C_{nt}^{+} = C_{nt}^{-} = \frac{-j\pi^2}{H^2\lambda_0 E_0^2(H)}\left(\frac{\epsilon_1\epsilon_2}{\epsilon_1+\epsilon_2}\frac{Z_t}{Z_0}\frac{B}{H}\alpha_e\right) \cdot\frac{E_t(x_b)E_J\left(\frac{b}{2}\right)}{2\ln\left[r_B(3)/r_A(3)\right]}. \tag{16}$$

For $i=1$, $j=1$, we have

$$C_{nt}^{-} = \frac{-j\pi^2}{h^2\lambda_0 E_0^2(h)}\left(\frac{-\epsilon_1\epsilon_2}{\epsilon_1+\epsilon_2}\frac{Z_t}{Z_0}\frac{b}{h}\alpha_e + \frac{Z_0}{Z_J}\frac{h}{b}\alpha_m\right) \cdot\frac{E_t\left(\frac{b}{2}\right)E_J\left(\frac{b}{2}\right)}{2\ln\left[r_B(1)/r_A(1)\right]}. \tag{17}$$

For $i=5,6$ and $j=4$, we have

$$C_{nt}^{+} = C_{nt}^{-} = \frac{-j\pi^2}{H^2\lambda_0 E_0^2(H)}\left(\frac{\epsilon_1\epsilon_2}{\epsilon_1+\epsilon_2}\right) \cdot\frac{Z_t}{Z_0}\frac{B}{H}\alpha_e\frac{E_t(x_b)E_J(x_a)}{2\ln\left[r_B(3)/r_A(3)\right]}. \tag{18}$$

For $i=6$ and $j=6$, we have

$$C_{nt}^{-} = \frac{-j\pi^2}{H^2\lambda_0 E_0^2(H)}\left(\frac{\epsilon_1\epsilon_2}{\epsilon_1+\epsilon_2}\frac{Z_t}{Z_0}\frac{B}{H}\alpha_e + \frac{Z_0}{Z_J}\frac{H}{B}\alpha_m\right) \cdot\frac{E_t(x_b)E_J(x_b)}{2\ln\left[r_B(3)/r_A(3)\right]}. \tag{19}$$

Other cases can be calculated accordingly.

V. S Parameters of Six-Port Network

Once $C_{nt}^{\pm}$ are determined for each transmission line, one can substitute them into (2) and calculate the S parameters. The S-parameters are related to $C_{nt}^{\pm}$ by

$$S_{ij} = \frac{V_t}{V_J} = \frac{h_t}{h_J}\left(\frac{\epsilon_r(i)}{\epsilon_r(j)}\right)^{1/4}\frac{E_0(i)}{E_0(j)}\sqrt{\frac{h_t b_J}{b_t h_J}}\,C_{nt}^{\pm}. \tag{20}$$

Assuming $Z_3 = Z_4 = Z_A$ and $Z_5 = Z_6 = Z_B$, the S parameters are summarized as

$$S_{11} = S_{22} = \frac{-j\pi}{h^2\lambda_0}\left(\frac{-\epsilon_1\epsilon_2}{\epsilon_1+\epsilon_2}\frac{b}{h}\frac{Z_1}{Z_0}\alpha_e + \frac{Z_0}{Z_1}\frac{h}{b}\alpha_m\right) \cdot\frac{1}{\left[r_1\left(\frac{b}{2}\right)+1\right]^2}\frac{\pi}{2\ln\left(r_B(1)/r_A(1)\right)}$$

$$S_{31} = \frac{-j\pi}{H^2\lambda_0}\left(\frac{\epsilon_1\epsilon_2}{\epsilon_1+\epsilon_2}\frac{Z_A}{Z_0}\frac{A}{h}\alpha_e + \frac{Z_0}{Z_1}\frac{H}{b}\alpha_m\right) \cdot\frac{\left(\frac{H}{h}\frac{b}{A}\right)^{1/2}\left(\frac{\epsilon_2}{\epsilon_1}\right)^{1/4}}{\left[r_3(x_a)+1\right]\left[r_1\left(\frac{b}{2}\right)+1\right]}\frac{\pi}{2\ln\left(r_B(2)/r_A(2)\right)}$$

$$S_{41} = \frac{-j\pi}{H^2\lambda_0}\left(\frac{\epsilon_1\epsilon_2}{\epsilon_1+\epsilon_2}\frac{Z_A}{Z_0}\frac{A}{h}\alpha_e - \frac{Z_0}{Z_1}\frac{H}{b}\alpha_m\right) \cdot\frac{\left(\frac{H}{h}\frac{b}{A}\right)^{1/2}\left(\frac{\epsilon_2}{\epsilon_1}\right)^{1/4}}{\left[r_4(x_a)+1\right]\left[r_1\left(\frac{b}{2}\right)+1\right]}\frac{\pi}{2\ln\left(r_B(2)/r_A(2)\right)}$$

$$S_{51} = S_{61} = \frac{-j\pi}{H^2\lambda_0}\frac{\epsilon_1\epsilon_2}{\epsilon_1+\epsilon_2}\frac{Z_B}{Z_0}\frac{B}{h}\alpha_e \cdot\frac{\left(\frac{H}{h}\frac{b}{B}\right)^{1/2}\left(\frac{\epsilon_2}{\epsilon_1}\right)^{1/4}}{\left[r_5(x_b)+1\right]\left[r_1\left(\frac{b}{2}\right)+1\right]}\frac{\pi}{2\ln\left(r_B(3)/r_A(3)\right)}$$

$$S_{44} = S_{33} = \frac{-j\pi}{H^2\lambda_0}\left(\frac{-\epsilon_1\epsilon_2}{\epsilon_1+\epsilon_2}\frac{Z_A}{Z_0}\frac{A}{H}\alpha_e + \frac{Z_0}{Z_A}\frac{H}{A}\alpha_m\right) \cdot\frac{1}{\left[r_4(x_a)+1\right]^2}\cdot\frac{\pi}{2\ln\left(r_B(2)/r_A(2)\right)}$$

$$S_{54} = S_{64} = \frac{-j\pi}{H^2\lambda_0}\frac{\epsilon_1\epsilon_2}{\epsilon_1+\epsilon_2}\frac{Z_B}{Z_0}\frac{B}{H}\alpha_e \cdot \frac{\left(\frac{A}{B}\right)^{1/2}}{[r_5(x_b)+1][r_4(x_a)+1]}\frac{\pi}{2\ln(r_B(3)/r_A(3))}$$

$$S_{66} = S_{55} = \frac{-j\pi}{H^2\lambda_0}\left(\frac{-\epsilon_1\epsilon_2}{\epsilon_1+\epsilon_2}\frac{Z_B}{Z_0}\frac{B}{H}\alpha_e + \frac{Z_0}{Z_B}\frac{H}{B}\alpha_m\right) \cdot \frac{1}{[r_6(x_b)+1]^2}\frac{\pi}{2\ln(r_B(3)/r_A(3))}.$$

The through-arm S parameters, such as S_{21}, S_{34}, and S_{56}, are more difficult to find since a part of through-wave exists. Instead, these parameters are deduced from the properties of the lossless network and the field symmetry. For a reciprocal, lossless circuit, the following equations hold:

$$[S^t][S]^* = [U] \tag{21}$$

and

$$S_{ij} = S_{ji}. \tag{22}$$

From the field symmetry, we have

$$S_{11} = S_{22} \qquad S_{33} = S_{44} \qquad S_{55} = S_{66} \qquad S_{32} = S_{41}$$
$$S_{63} = S_{64} = S_{53} = S_{54}$$
$$S_{51} = S_{52} = S_{61} = S_{62}.$$

Therefore, the S-parameter matrix becomes

$$[S] = \begin{pmatrix} S_{11} & S_{21} & S_{31} & S_{41} & S_{51} & S_{51} \\ S_{21} & S_{11} & S_{41} & S_{31} & S_{51} & S_{51} \\ S_{31} & S_{41} & S_{33} & S_{34} & S_{54} & S_{54} \\ S_{41} & S_{31} & S_{34} & S_{33} & S_{54} & S_{54} \\ S_{51} & S_{51} & S_{54} & S_{54} & S_{55} & S_{56} \\ S_{51} & S_{51} & S_{54} & S_{54} & S_{56} & S_{55} \end{pmatrix}. \tag{23}$$

The remaining parameters S_{21}, S_{34}, and S_{56} can be found from (21). The results are summarized below:

$$|S_{21}| = \left(1 - |S_{11}|^2 - |S_{31}|^2 - |S_{41}|^2 - 2|S_{51}|^2\right)^{1/2}$$

and

$$\theta_{21} = \theta_{11} + \cos^{-1}\left[\frac{-S_{31}S_{41}^* + S_{41}S_{31}^* + 2|S_{51}|^2}{2|S_{11}S_{21}|}\right]$$

$$|S_{34}| = \left(1 - |S_{31}|^2 - |S_{41}|^2 - |S_{33}|^2 - 2|S_{54}|^2\right)^{1/2}$$

and

$$\theta_{34} = \theta_{44} + \cos^{-1}\left[\frac{-\left(S_{31}S_{41}^* + S_{41}S_{31}^* + 2|S_{54}|^2\right)}{2|S_{33}S_{34}|}\right]$$

$$|S_{56}| = \left(1 - 2|S_{51}|^2 - 2|S_{54}|^2 - |S_{55}|^2\right)^{1/2}$$

$$\theta_{56} = \theta_{55} + \cos^{-1}\left[\frac{-\left(|S_{51}|^2 + |S_{54}|^2\right)}{|S_{55}S_{56}|}\right].$$

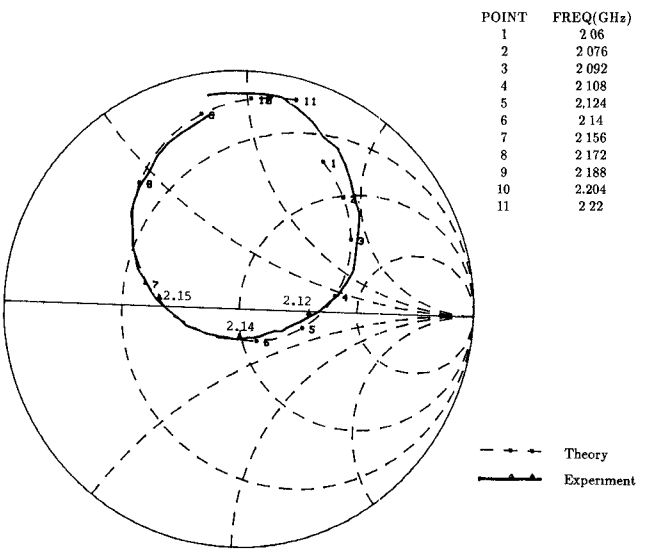

Fig. 4. Comparison of calculated and experimental results [17] for input impedance as a function of frequency. The circuit has the following parameters:

$R = 4.6$ mm	$x_b = 19.6$ mm
$A = 30$ mm	$b = 4.7$ mm
$B = 39.2$ mm	$h = 1.6$ mm
$\epsilon_1 = 2.55$	$H = 1.6$ mm
$\epsilon_2 = 2.55$	$t = 0.3$ mm
$x_a = 15$ mm	$L_1 = 12$ mm
	$L_0 = 120$ mm.

VI. Results and Discussion

A computer program was written to facilitate the calculation based upon the S parameters and the connected scattered matrix method [13]. The patch antenna terminated load Y_A (or Y_B) can be represented by

$$Y = G + jB_d = G_r + G_m + jB_d. \tag{24}$$

G_r is the radiation admittance, which is given by an approximate formula in [14]. The mutual conductance (G_m) due to the patch radiation ends is given in [15]. The susceptance B_d can be found in [16]. The resultant theoretical and experimental input impedances as a function of frequency are shown in Figs. 4 and 5 for comparison. It can be seen that the agreement is very good.

To examine the effects of different parameters, all parameters will be kept the same as in Fig. 4 except that one parameter is changed each time. The input impedances for different sizes of aperture radius are shown in Fig. 6 as a function of frequency. It can be seen that the impedance levels are quite sensitive to the aperture size. Only narrow-band matching can be accomplished.

It is interesting to compare our results for a circular aperture with those given by Sullivan and Schaubert for a rectangular aperture [6]. As the radius of aperture increases, the radius of the impedance circle increases and the resonant frequency (i.e., the frequency with minimum reflection) decreases. These are similar to the results given in [6, figs. 5 and 6] using the length of slot as a variable. The center location of each impedance circle is shifted due to the fact that the reference plane used in our analysis is

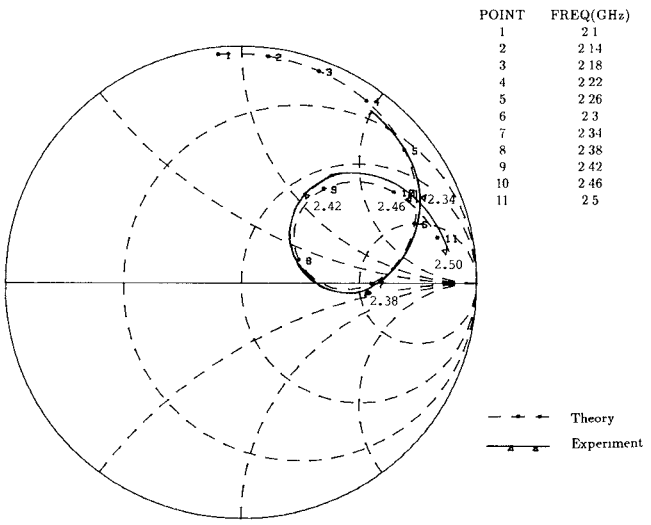

Fig. 5. Comparison of calculated and experimental input impedances as a function of frequency. The circuit has the same parameters as in Fig. 4 except that $\epsilon_1 = \epsilon_2 = 2.24$, $h = H = 1.75$ mm, $t = 0.84$ mm, and $L_0 = 76$ mm.

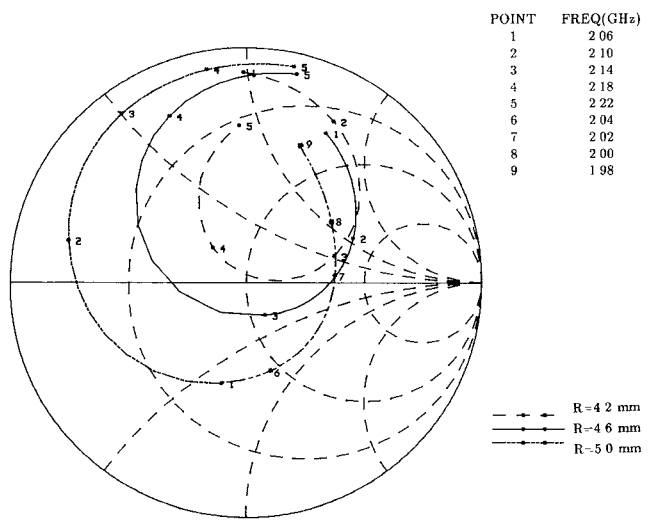

Fig. 6. Input impedance for different sizes of apertures as a function of frequency. All other parameters are the same as in Fig. 4.

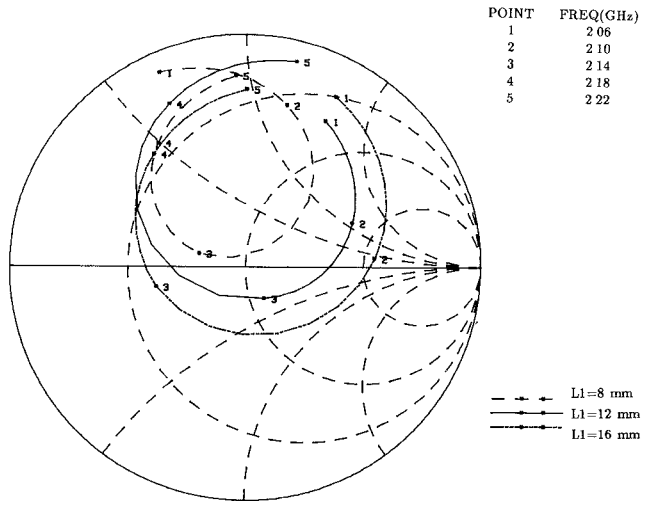

Fig. 7. Input impedance as a function of frequency for different values of L_1. All other parameters are the same as in Fig. 4.

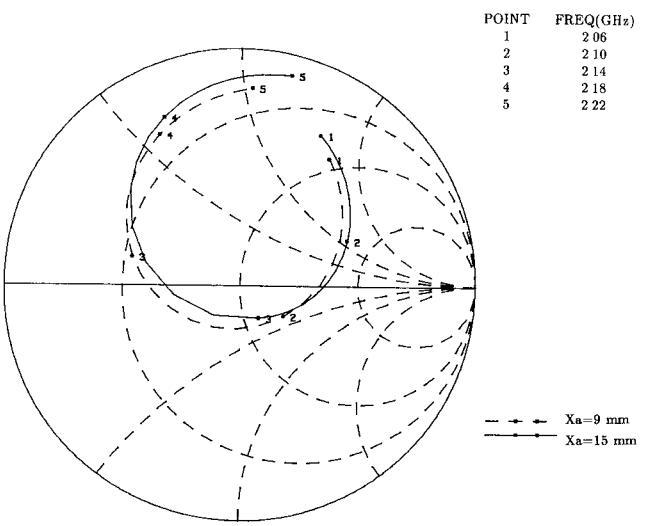

Fig. 8. Input impedance as a function of frequency for different locations of x_a. All other parameters are the same as in Fig. 4.

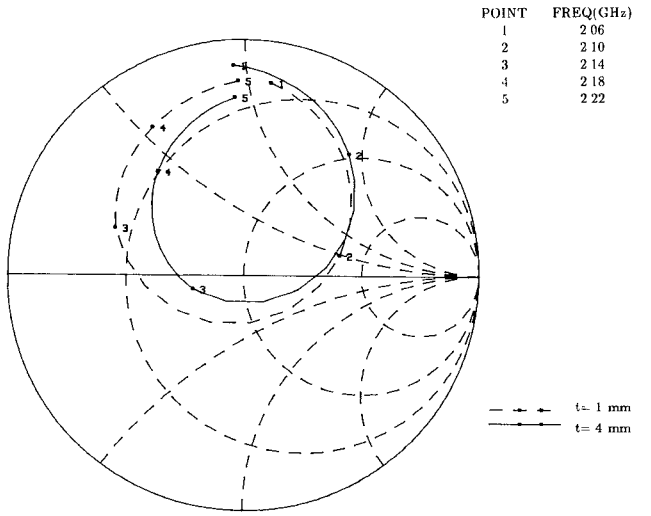

Fig. 9. Input impedance as a function of frequency for different ground plane thicknesses. All other parameters are the same as in Fig. 4.

taken at a distance L_0 from the aperture center. From these results, it can be seen that the design of the aperture size is critical in achieving impedance matching at the operating frequency.

In the actual design, the open stub L_1 can be used to facilitate the impedance matching. Fig. 7 shows the input impedance as a function of frequency for different lengths of L_1. It can be seen that the selection of $L_1 = 9$ mm gives the best matching at around 2.1 GHz. When L_1 decreases, the radius of the impedance circle decreases and the center location of the impedance circle is shifted counterclockwise. These are consistent with the results by Sullivan and Schaubert for a rectangular aperture case [6, fig. 4]. The differences of the curve trends between the two analyses are mainly due to the different reference planes used and the different shapes of the apertures analyzed.

The effects of the aperture location were also investigated. Fig. 8 shows the input impedance as a function of

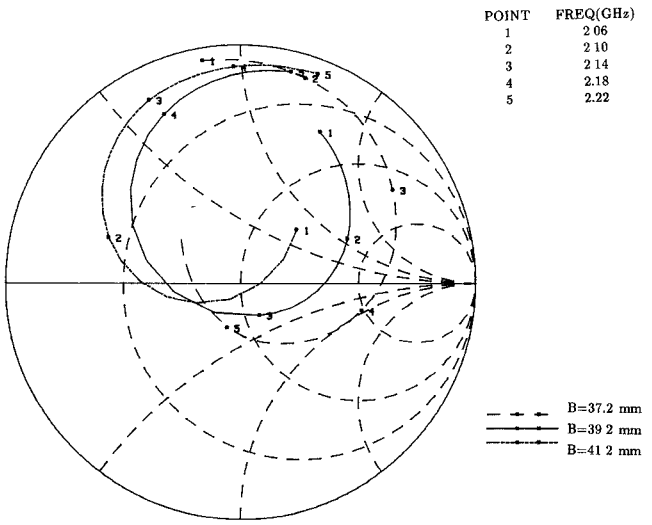

Fig. 10. Input impedance as a function of frequency for different patch antenna lengths. All other parameters are the same as in Fig. 4.

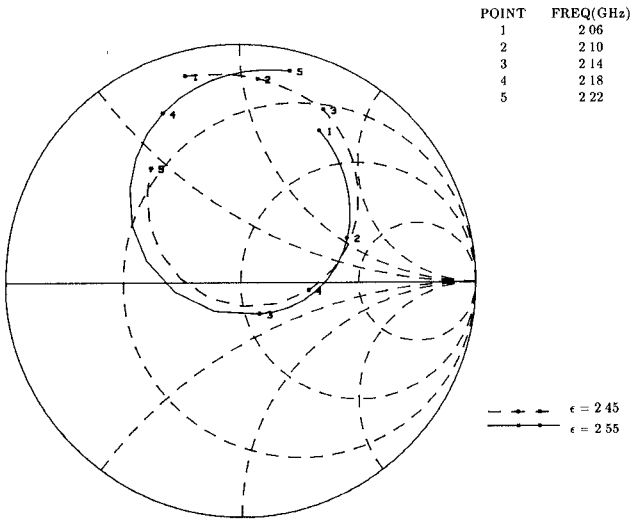

Fig. 11. Input impedance as a function of frequency for different substrate dielectric constants. $\epsilon_1 = \epsilon_2 = 2.45$ and 2.55. All other parameters are the same as in Fig. 4.

frequency for different values of x_a. The effects are not as significant as the aperture size and the open stub length. Similar results can be obtained for different values of x_b.

The ground plane thickness has little effect on the input impedance and the input reflection coefficient. The results are shown in Fig. 9 for different values of t.

Another parameter which has strong effects on the input impedance is the dimension of the patch length. Fig. 10 shows the effects of this dimension on the input impedance as a function of frequency. It can be seen that the length of the patch antenna (B) is slightly shorter than the half-wavelength at the operating frequency. As expected, the resonant frequency is increased as B dimension is decreased.

The substrate dielectric constant also has strong effects on the design. Fig. 11 shows that the resultant input impedance could change somewhat even with a slightly different substrate dielectric constant. The dielectric constant affects many design parameters, including the line characteristic impedance, the coupling coefficient, the stub length, and the patch dimensions. In general, it is not easy to adjust for matching purposes.

From the above results, the input impedance matching can be most effectively achieved by adjusting the open stub length (L_1) and the aperture radius (R). The patch length is designed slightly shorter than half a wavelength. The ground plane thickness and the aperture location have little effect and the substrate dielectric constant is generally difficult to adjust. However, these parameters should be initially designed properly at the operating frequency.

VII. Conclusions

An analysis has been developed to model the equivalent circuit of a microstrip line coupled to a microstrip patch antenna using a circular aperture. The analysis is based on the aperture coupling theory and the six-port S-parameter matrix derivation. The input impedance can be easily calculated from the S-parameter matrix. The circuits should have many applications in hybrid and monolithic active arrays.

Appendix

For a large aperture, the electric and magnetic fields are no longer constant. For better accuracy, a field average factor is introduced in the calculation of polarizability α_e or α_m.

$A(E_i, E_j)$ is the average factor of the electric field for a large aperture. $A(E_i, E_j)$ is defined as

$$A(E_i, E_j) = CA(E_i)A(E_j). \tag{A1}$$

E_i is the scattered electric field and E_j is the incident field. C is a constant to be determined. The average factor of scattered electric field can be given by

$$A(E_i) = \frac{\bar{E}_i}{E_i(x_a)}. \tag{A2}$$

Similarly, for the incident field,

$$A(E_j) = \frac{\bar{E}_j}{E_j(x_a)}. \tag{A3}$$

For an aperture with radius R as shown in Fig. 12, the average field $\bar{E}_i$ can be found by

$$\bar{E}_i = \frac{1}{\pi R^2}\int_s E(x, z)\, ds. \tag{A4}$$

Neglecting the phase difference of the field in the z direction for an aperture small compared to the wavelength, the integration in (A4) can be carried out by dividing the aperture into three regions, as shown in Fig. 12.

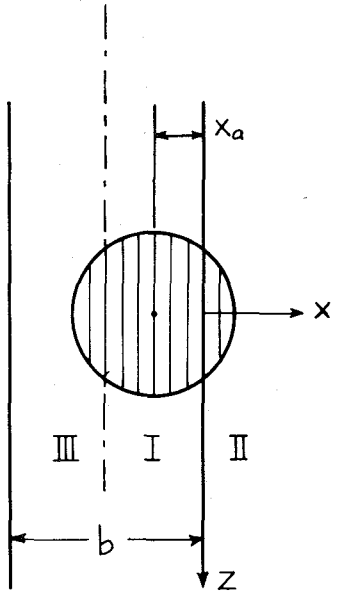

Fig. 12. Field averaging on aperture.

Using the results from conformal mapping, we have

$$z = \left[R^2 - (x + x_a)^2\right]^{1/2}$$

$$E(x) = E_0/[r(x)+1]$$

$$r(x) = \begin{cases} r(x) & \text{in regions I and II} \\ r(-b-x) & \text{in region III.} \end{cases}$$

Then

$$\int E(x,z)\,ds = \int E(x)z(x)\,dx$$

$$= 2\left[\int_0^{-b/2} E(x)z(x)\,dx + \int_0^{R-x_a} E(x)z(x)\,dx + \int_{\frac{-b}{2}}^{-(R+x_a)} E(x)z(x)\,dx\right]. \quad \text{(A5)}$$

The factor 2 is due to the fact that only half area ($z(x) > 0$) is taken in the integration. If the region is divided into N strips, $A(E_i)$ can be given simply by

$$A(E_i) = \frac{4[r(x_a)+1]}{N\pi R} \sum_{i=1}^{N} \frac{\left[R^2 - (x_i + x_a)^2\right]^{1/2}}{r(x_i)+1}. \quad \text{(A6)}$$

$A(E_j)$ can be found similarly. Since the average factor of the field over the aperture does not include the effects of coupled scattered coefficients, an additional correction factor C is introduced. C can be determined by forcing the reflection coefficient at the input port equal to 1 with all other ports terminated by a variable short circuit.

$A(H_i, H_j)$ can be taken as $A(E_i, E_j)$ since the electric field is proportional to the magnetic field.

Acknowledgment

The authors would like to thank F. Wang, J. Klein, and K. Hummer for many helpful discussions and technical assistance.

References

[1] K. Chang, *Millimeter-wave Planar Integrated Circuits and Subsystems*, vol. 14 of Infrared and Millimeter-Waves, K. Button, Ed. New York: Academic Press, 1985, pp. 79–187.

[2] K. Chang *et al.*, "*W*-band (75–110 GHz) microstrip components," *IEEE Trans. Microwave Theory Tech.*, vol. MTT-33, pp. 1375–1382, Dec. 1985.

[3] D. Pozar and D. H. Schaubert, "Comparison of architectures for monolithic phased array antennas," *Microwave J.* pp. 93–104, Mar. 1986.

[4] J. W. Mink, "Quasi-optical power combining of solid-state millimeter-wave sources," *IEEE Trans. Microwave Theory Tech.*, vol. MTT-34, pp. 273–279, Feb. 1986.

[5] K. Chang and C. Sun, "Millimeter-wave power combining techniques," *IEEE Trans. Microwave Theory Tech.*, vol. MTT-31, pp. 91–105, Feb. 1983.

[6] P. L. Sullivan and D. H. Schaubert, "Analysis of an aperture coupled microstrip antenna," *IEEE Trans. Antennas Propagat.*, vol AP-34, pp. 977–984, Aug. 1986.

[7] D. M. Pozar, "A reciprocity method of analysis for printed slot and slot coupled microstrip antennas," *IEEE Trans. Antennas Propagat.*, vol. AP-34, pp. 1439–1446, Dec. 1986.

[8] F. Assadourian and E. Rimai, "Simplified theory of microstrip transmission systems," *Proc. IRE*, pp. 1651–1657, Dec. 1952.

[9] D. James, G. R. Painchaud, and W. J. R. Hoefer, "Aperture coupling between microstrip and resonant cavities," *IEEE Trans. Microwave Theory Tech.*, vol. MTT-25, pp. 392–398, May 1977.

[10] J. Miao and T. Itoh, "Coupling between microstrip line and image guide through small apertures in the common ground plane," *IEEE Trans. Microwave Theory Tech.*, vol. MTT-31, pp. 361–363, Apr. 1983.

[11] R. Levy, "Improved single and multiaperture waveguide coupling theory, including explanation of mutual interactions," *IEEE Trans. Microwave Theory Tech.*, vol. MTT-28, pp. 331–338, Apr. 1980.

[12] R. E. Collin, *Foundations for Microwave Engineering.* New York: McGraw-Hill, pp. 183–197.

[13] K. C. Gupta, R. Garg, and R. Chadha, *Computer-Aided Design of Microwave Circuits.* Dedham, MA: Artech House, 1981, ch. 11.

[14] C. Wood *et al.*, "Radiation conductance of open-circuit low dielectric constant microstrip," *Electron. Lett.* vol. 14, pp. 121–123, 1978.

[15] J. R. James *et al.*, *Microstrip Antenna Theory and Design.* London: Peter Peregrinus, 1981, pp. 88–93.

[16] P. Bhartia and I. Bahl, *Millimeter Wave Engineering and Applications.* New York: Wiley, 1984, ch. 9.

[17] D. M. Pozar, "Microstrip antenna aperture-coupled to a microstripline," *Electron. Lett.*, vol. 17, pp. 49–50, Jan. 1985.

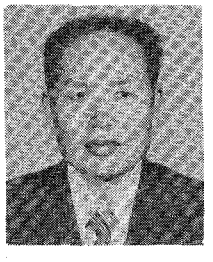

Xuanzheng Gao was born in Wuchan, China, on October 5, 1936. He graduated at Wuchan University in 1962, and since then has done research on microwaves and antennas at the Xian Radio Technology Institute. He was a Visiting Scholar at the Electrical Engineering Department, Texas A & M University, from Sept. 1985 to Aug. 1987.

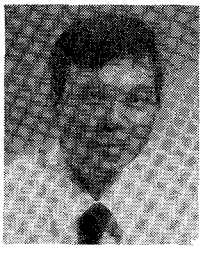

Kai Chang (S'75–M'76'–SM'85) received the B.S.E.E. degree from National Taiwan University, Taipei, Taiwan in 1970, the M.S. degree from the State University of New York at Stony Brook in 1972, and the Ph.D. degree from the University of Michigan, Ann Arbor, in 1976.

From 1972 to 1976 he worked for the Microwave Solid-State Circuits Group, Cooley Electronics Laboratory of the University of Michigan as research assistant. From 1976 to 1978 he was employed by Shared Applications, Ann Arbor,

where he worked in computer simulation of microwave circuits and microwave tubes. From 1978 to 1981, he worked for the Electron Dynamic Division, Hughes Aircraft Company, Torrance, CA, where he was involved in the research and development of millimeter-wave devices and circuits. This activity resulted in state-of-the-art IMPATT oscillator and power combiner performance at 94, 140, and 217 GHz. Other activities included silicon and gallium arsenide IMPATT diode design and computer simulation, Gunn oscillator development, and monopulse comparator and phase shifter development. From 1981 to 1985 he worked for TRW Electronics and Defense, Redondo Beach, CA, as a Section Head in the Millimeter-Wave Technology Department, developing state-of-the-art millimeter-wave integrated circuits and subsystems including mixers, Gunn VCO's, IMPATT transmitters and amplifiers, modulators, upconverters, switches, multipliers, receivers, and transceivers. In August 1985, he joined the Electrical Engineering Department of Texas A & M University as an Associate Professor. His current interests are in microwave and millimeter-wave devices and circuits, microwave-optic interactions, and radar systems.

Dr. Chang serves as the editor of the *Handbook of Microwave and Optical Components*, to be published by Wiley & Sons, Inc. He has published over 70 technical papers in the areas of microwave and millimeter-wave devices and circuits.